Quantum and Classical Temporal Correlations in (1+1)D Quantum Cellular Automata

Edward Gillman,[1,2] Federico Carollo,[3] and Igor Lesanovsky[1,2,3]

[1]School of Physics and Astronomy, University of Nottingham, Nottingham NG7 2RD, United Kingdom
[2]Centre for the Mathematics and Theoretical Physics of Quantum Non-Equilibrium Systems, University of Nottingham, Nottingham NG7 2RD, United Kingdom
[3]Institut für Theoretische Physik, Universität Tübingen, Auf der Morgenstelle 14, 72076 Tübingen, Germany

(Received 27 April 2021; accepted 5 November 2021; published 1 December 2021)

We employ (1 + 1)-dimensional quantum cellular automata to study the evolution of entanglement and coherence near criticality in quantum systems that display nonequilibrium steady-state phase transitions. This construction permits direct access to the entire space-time structure of the underlying nonequilibrium dynamics, and allows for the analysis of unconventional correlations, such as entanglement in the time direction between the "present" and the "past." We show how the uniquely quantum part of these correlations—the coherence—can be isolated and that, close to criticality, its dynamics displays a universal power-law behavior on approach to stationarity. Focusing on quantum generalizations of classical nonequilibrium systems: the Domany-Kinzel cellular automaton and the Bagnoli-Boccara-Rechtman model, we estimate the universal critical exponents for both the entanglement and coherence. As these models belong to the one-dimensional directed percolation universality class, the latter provides a key new critical exponent, one that is unique to quantum systems.

DOI: 10.1103/PhysRevLett.127.230502

Introduction.—Cellular automata (CA) are paradigmatic models for the study of nonequilibrium processes [1–3] that also serve as models of computation [4,5]. An important class of CA are so-called (1 + 1)-dimensional CA [6]. These are two-dimensional (2D) lattice models whose evolution is such that the state of a given row depends only on the row above it. This results in the emergence of an effective time dimension, see Fig. 1(a). The dynamics of CA follow simple local update rules that propagate the state along the time dimension. This allows the implementation of a whole host of nonequilibrium processes, including some that display phase transitions into absorbing states. In the classical setting this construction has enabled the accurate study of nonequilibrium universality classes, such as that of directed percolation (DP) [7]. Here, sampling the dynamics of a suitably chosen order parameter enables the extraction of critical exponents. Importantly, these exponents are universal and also apply to other physical processes. For example, DP universality is also found in water percolating through sand [6], the dynamics of epidemic spreading [8], or even electroconvection in nematic liquid crystals [9] and the transition to turbulence [10]. Very recently, it was shown that also other quantities, that are not accessible by sampling—such as entropies—show critical behavior and are found to obey universal power-law scaling [11]. This raises the question as to whether there might be additional exponents, beyond the ones of the order parameter or correlation functions, that characterize universality classes.

Considerable activity is dedicated to generalizing the CA concept into the quantum domain, often looking at computational applications [12–16]. With regards to (1 + 1)D CA, the framework introduced in Refs. [17,18] provides a generalization to a 2D quantum lattice system.

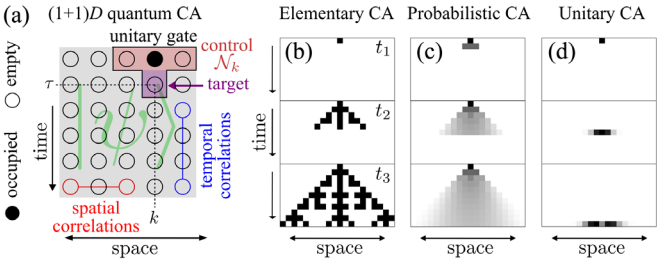

FIG. 1. (1 + 1)D quantum cellular automata. (a) (1 + 1)D QCA are based on the successive application of unitary quantum gates. By acting on pairs of rows sequentially, an entangled 2D quantum state $|\psi\rangle$ is created that encodes the entire space-time structure of the ensuing non-equilibrium dynamics. (b) An elementary cellular automaton (ECA) generates a 2D product state. On the QCA an ECA can be realized by gates that merely flip the unoccupied target sites into occupied ones. The image shows snapshots taken at three times ($t_1 < t_2 < t_3$) for an evolution under rule 150, see Table I. (c) An evolution similar to a probabilistic classical CA is implemented when the gate rotates target sites into superposition states. This generates an entangled 2D quantum state. The image shows the density of occupied sites of the BBR model. (d) Unitary evolution of a 1D system in the (1 + 1)D QCA framework, for comparison. Here, the space-time structure for this process is inaccessible.

These $(1+1)$D quantum cellular automata (QCA) can be constructed to include $(1+1)$D CA as a special case, providing a natural starting point for investigations into the impact of quantum correlations on nonequilibrium processes and nonequilibrium phase transitions (NEPTs)—a topic of substantial research efforts in its own right [17,19–25]. Interestingly, $(1+1)$D QCA can be regarded as manifestations of quantum feed-forward neural networks [26] and are realizable on current quantum simulation platforms, such as two-dimensional Rydberg lattice gases [27–30].

In this work we exploit the $(1+1)$D QCA structure that encodes an entire space-time dynamics within a single pure 2D quantum state. In such a structure, correlations in the temporal (vertical) dimension can be studied in a well-defined manner, by partitioning the 2D lattice along a row, see Fig. 1(a). This allows one to study the nonequilibrium behavior of a wide variety of novel and interesting quantities. Specifically, we consider the temporal entanglement quantified by the second-order Renyi-entropy, S_2. In that case, one arrives exactly at the nonequilibrium entropy considered in Ref. [11] (see Ref. [31] for a review of entanglement and entropy). Furthermore, we consider the contribution to the entropy stemming from quantum coherences, C_2, which can be isolated in this case. This quantity is strictly zero in the classical model, and thus constitutes an essential quantity in understanding the uniquely quantum aspects of NEPTs.

Throughout, we focus on QCA related to quantum generalizations of two paradigmatic nonequilibrium models: the Domany-Kinzel cellular automaton (DKCA) [7] and the Bagnoli-Boccara-Rechtman (BBR) model [32]. Both systems possess a critical point associated with an absorbing phase transition (APT). By construction, these quantum models reproduce the observables of their classical counterparts. Therefore, they belong to the 1D DP universality class and S_2 displays a universal power-law scaling on its approach to stationarity [11]. In $(1+1)$D QCA this can be understood as the universal scaling of temporal entanglement. Moreover, when considering the behavior of C_2, we again find that this quantity displays a power-law decay. Not only does this show that at criticality quantum effects persist on a timescale longer than any microscopic one, but also that the uniquely quantum aspects of APTs are universal and can be quantified, and we provide novel estimates of the corresponding critical exponent to this end.

$(1+1)$D *QCA and link to other CA models.*—QCA are lattice systems with sites that may be either occupied or empty; see Fig. 1(a). The dynamics is constructed such that the occupation of sites in a row—or more generally in a d-dimensional surface—is determined by those of the row above it [17,18]. This leads to an effective time dimension, and the corresponding models are termed $(d+1)$-dimensional with d spatial dimensions perpendicular to the single "time" dimension [6]. Similar models have been studied extensively in the context of classical systems [33]. In $(1+1)$D QCA, at any time t the system is described by a pure quantum state $|\psi_t\rangle$, which is an element of the Hilbert space $\mathcal{H}=\bigotimes_{\tau,k}\mathcal{H}_{\tau,k}$, where $\mathcal{H}_{\tau,k}$ are local Hilbert spaces of a 2D lattice indexed by $(\tau,\ k)$. Here we consider local Hilbert spaces that are two dimensional with basis $\{|\circ\rangle, |\bullet\rangle\}$, where $n|\circ\rangle = 0$, $n|\bullet\rangle = |\bullet\rangle$ and n is the local particle number operator. We will refer to the states $|\circ\rangle$ and $|\bullet\rangle$ as occupied and empty, respectively.

The $(1+1)$D QCA evolves under the action of unitary gates $G_{\tau,k}$. These apply local updates to a "target" site at (τ,k), depending on the state of a set of "control" sites in row $\tau-1$ that form the "neighborhood," $\mathcal{N}_k$, of site k, see Fig. 1(a). Since we are considering binary variables, $\mathcal{N}_k$ is taken to be an integer labeling the possible neighborhoods, whose binary representation (see Table I) specifies the occupation of the sites [5]. The state $|\psi_t\rangle$ evolves in discrete time-steps as $|\psi_t\rangle = \mathcal{G}_t|\psi_{t-1}\rangle$. Here the "global update" $\mathcal{G}_t$ consists of an ordered product of $G_{t,k}$, one per each site of row t. We will consider the situation in which the 2D state is initialized at $t=1$ into a product state of all unoccupied sites, $|\circ\rangle$, except for the first row, $\tau=1$. This will have a single occupied site, $|\bullet\rangle$, at the center, which we refer to as the seed initial condition. During the subsequent evolution, $|\psi_t\rangle$ then encodes the entire space-time structure of cellular automaton dynamics from this initial condition, i.e., it allows for access to the full history of trajectories, permitting the analysis of typically inaccessible (quantum) correlations between different space-time regions.

The $(1+1)$D QCA framework generalizes classical cellular automata (CCA) into a unitary quantum setting. It includes canonical classical models, such as deterministic CCA—, e.g., the much-studied elementary cellular automata (ECA) [4,5]—and classical probabilistic cellular automata (PCA), such as those studied in the context of APTs [6], as limiting cases [see Figs. 1(b) and 1(c)]. Moreover, 1D unitary CAs, as discussed in, e.g., Refs. [15,16] can also be represented as $(1+1)$D QCA. However, as illustrated in Fig. 1(d), such an evolution generates an "effectively" 1D quantum state, which is

TABLE I. *Local update rules for* $(1+1)$D *QCA*. The gate (1) is defined by eight values of the probability $p(\mathcal{N})$, one for each possible configuration of the neighbourhood $\mathcal{N}$ [see Fig. 1(a)]. The three examples given encode the classical ECA rule 150, the DKCA and BBR model. The totalistic nature of the updates for the DKCA and BBR model results in only two parameters p_1 and p_2. See also Fig. 1(b) and (c) for the evolution of an initial seed generated by the ECA and BBR rules.

$\mathcal{N}$	$\bullet\bullet\bullet$	$\bullet\bullet\circ$	$\bullet\circ\bullet$	$\bullet\circ\circ$	$\circ\bullet\bullet$	$\circ\bullet\circ$	$\circ\circ\bullet$	$\circ\circ\circ$
ECA	1	0	0	1	0	1	1	0
DKCA	p_2	p_1	p_2	p_1	p_1	0	p_1	0
BBR	1	p_2	p_2	p_1	p_2	p_1	p_1	0

shifted along the time direction using SWAP gates (see Ref. [34]).

In the following, we consider gates that act on a single target site and a three-site "control" neighborhood with the form,

$$G_{\tau,k}|\circ\rangle = \sum_{\mathcal{N}_k} P_{\mathcal{N}_k} \otimes e^{-i\sigma_x \alpha(\mathcal{N}_k)}|\circ\rangle. \tag{1}$$

The symbol $\otimes$ separates the operators which act on the controls (placed to the left) and on the target (placed on the right): the $P_{\mathcal{N}_k} = |\mathcal{N}_k\rangle\langle\mathcal{N}_k|$ are projectors onto the different "classical" configurations of the control sites [see Fig. 1(a) and Table I] and $\sigma_x = |\circ\rangle\langle\bullet| + |\bullet\rangle\langle\circ|$ acts on the target site. The angles $\alpha(\mathcal{N}_k)$ determine by how much the target site is rotated from its initial state $|\circ\rangle$ into a superposition. The probability for the target site to be occupied, given a particular configuration of the control sites, is $P\{n_{\tau,k} = 1|\mathcal{N}_k\} = p(\mathcal{N}_k) = \sin^2[\alpha(\mathcal{N}_k)]$. For the gate (1), a local update (or "rule") is specified by choosing the eight (real) values of $\alpha(\mathcal{N}_k)$ or, equivalently, $p(\mathcal{N}_k)$. As we discuss in the following this includes several informative cases, listed in Table I, which directly connect to CCA with simultaneous updates. This is because for these cases the $G_{\tau,k}$ for different k commute, such that all choices of $\mathcal{G}_t$ are equivalent.

Choosing rotation angles such that $p(\mathcal{N}_k) = 0$, 1, the gate of Eq. (1) reproduces deterministic CCA on the 2D state $|\psi_t\rangle$, which remains in a product (unentangled) form at all times, see Fig. 1(b). For example, ECA can be realised in this setting including irreversible cases [5], which corresponds to the classical result that irreversible CCA can be embedded in higher-dimensional reversible CCA [35]. Further to that, Eq. (1), contains the case of classical PCA [see Fig. 1(c)]. Here the diagonal components of the density matrix $\Xi_t = |\psi_t\rangle\langle\psi_t|$ are equal to the probability of producing the corresponding space-time configuration under a PCA dynamics [17]. However, the unitary dynamics of the $(1+1)$D QCA can generate off-diagonal terms in Ξ_t, i.e., coherence. This means that the gate in Eq. (1) generalizes any desired PCA into a genuine quantum system: the $(1+1)$D QCA encodes the original classical dynamics, including all associated physics such as APTs, while also displaying uniquely quantum features. For example, the BBR model is a PCA with a three-site control neighbourhood that displays APTs [32,36]. It displays two absorbing states (the fully occupied and fully empty product states) and is totalistic, meaning that the local updates depend only on the total number of occupied sites in the neighbourhood, see Table I. The corresponding totalistic update rule with a two-site neighborhood, the DKCA, which displays a single absorbing state of all empty sites, can also be considered in this three-site neighborhood setting, e.g., by making updates not depending on the control site in the middle. As for deterministic CCA, $|\psi_t\rangle$ encodes also in this case the entire space-time history, although now being an entangled state, see Fig. 1(c).

Scaling of temporal correlations.—In the following, we will focus on $(1+1)$D QCA with gates as in Eq. (1), that realize quantum generalizations of the DKCA and the BBR model. We will refer to these as QDKCA and QBBR model, respectively. At any time, the QCA can be partitioned in such a way that the tth row is singled out. Since rows with $\tau > t$ are in a product state, the entanglement between the two subsystems generated by the partition quantifies the amount of quantum correlations in the pure state $|\psi_t\rangle$, between the "present" (sites in row t) and the "past" (rows $\tau < t$). We measure this "present-past" entanglement through the second-order Renyi entropy, i.e., the logarithm of the purity of the reduced state $\rho_t = \mathrm{Tr}_{\tau\neq t}\Xi_t$ of the tth row:

$$S_2(t) = -\ln \mathrm{Tr}[\rho_t^2]. \tag{2}$$

Given that we are considering extensions of PCA, it is natural to expand ρ_t into a diagonal part, ρ_t^{cl}, and an off-diagonal part, X_t, such that $\rho_t = \rho_t^{\mathrm{cl}} + X_t$. For classical processes all off-diagonal terms are zero and $\rho_t = \rho_t^{\mathrm{cl}}$ [11,34]. Under this decomposition the purity of the reduced state becomes a sum of two terms: $\mathrm{Tr}[\rho_t^2] = \mathrm{Tr}[(\rho_t^{\mathrm{cl}})^2] + C_2(\rho_t)$. The first one is equivalent to the classical component of the purity. This can be viewed as due to the probabilistic nature of the process through which sites can be rotated into the occupied state $|\bullet\rangle$. The second term

$$C_2(\rho) = \mathrm{Tr}[X^2] = \sum_{i,j} |X_{ij}|^2, \tag{3}$$

is the ℓ_2 norm of the density matrix coherence. This contribution is positive, and zero only if $\rho_t = \rho_t^{\mathrm{cl}}$. As such, it can only increase the purity of ρ_t and is a manifestation of the quantum correlations present in the QCA. While sufficient for our purposes, we note that C_2 is not a strict measure of coherence as it violates certain monotonicity conditions [37].

For some classical PCA, it was recently found that near the critical point of an ATP the second-order Renyi entropy scales as $S_2^{\mathrm{cl}} \sim t^{-p}$, with a universal exponent $p = 0.632\,613(6)$ [11]. The same behavior is expected, by construction, when considering ρ_t^{cl} of the QDKCA and the QBBR model, and hence

$$S_2^{\mathrm{cl}}(t) = -\ln \mathrm{Tr}[(\rho_t^{\mathrm{cl}})^2] \tag{4}$$

should display a power-law decay at criticality.

In what follows, we focus on the quantum Renyi entropy in Eq. (2) and show that, in the vicinity of the APT of the QDKCA and the QBBR model, it obeys a scaling form

$$S_2(t) \sim t^{-q_{\mathrm{ent}}}. \tag{5}$$

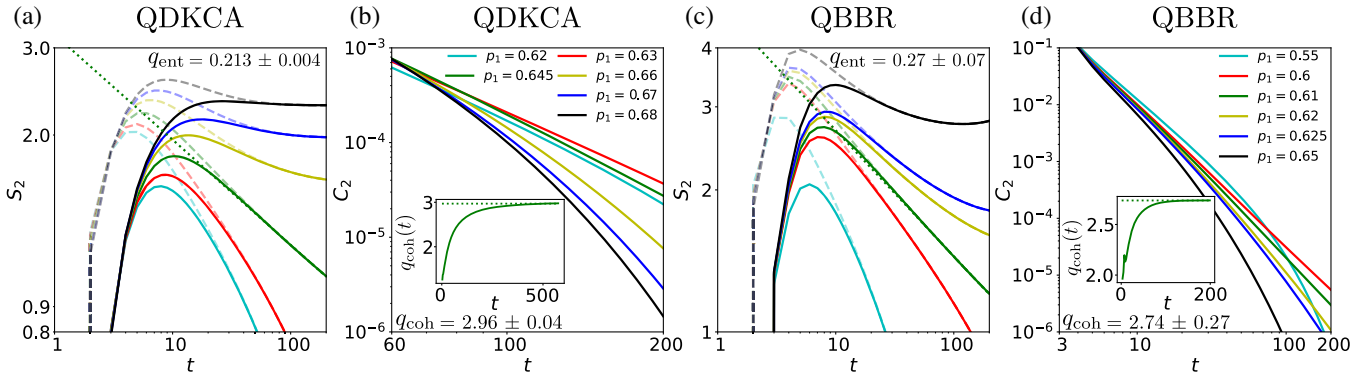

FIG. 2. Critical scaling of entanglement and coherence. (a) Dynamics of the second-order Renyi entropy S_2 (solid lines) for the QDKCA with $p_2 = 0.874$. MPSs with bond dimension $\chi = 128$ were used to simulate the dynamics of a lattice with $L = 256$ sites in the spatial direction. Six different values of p_1 [indicated in panel (b)] in the vicinity of the critical point were considered. For comparison we also display $S_2^{\rm cl}$ (dashed lines). For $p_1 = 0.645$, where the DKCA has a critical point [6], a power law is observed with exponent $q_{\rm ent} = 0.213 \pm 0.004$. See the text for more details on the estimation procedure and the Supplemental Material [34] for a discussion of error estimation. (b) C_2 for the QDKCA. At the critical point, $p_1 = 0.645$, a power-law behavior is observed. The corresponding exponent is estimated by calculating the effective exponent (see main text), shown in the inset, yielding $q_{\rm coh} = 2.96 \pm 0.04$. (c) S_2 for the QBBR model and $p_2 = 0.2$. For $p_1 = 0.61$, a power-law behavior with $q_{\rm ent} = 0.27 \pm 0.07$ can be observed. (d) C_2 for the QBBR model. At the critical point, $p_1 = 0.61$, power-law scaling with an exponent $q_{\rm coh} = 2.74 \pm 0.27$ is observed. The inset shows the time-dependent effective exponent at criticality.

Furthermore, we observe that the coherence also follows a similar power-law decay close to criticality,

$$C_2(t) \sim t^{-q_{\rm coh}}, \tag{6}$$

which defines an additional critical exponent $q_{\rm coh}$. For the seed initial conditions considered, we establish that $q_{\rm coh} \gg q_{\rm ent}$. As might then be expected, we find that the quantum entropy $S_2(t)$ tends to the one of the corresponding classical PCA, $S_2^{\rm cl}(t)$, for sufficiently long times.

Numerical results.—In the following we present results concerning the scaling of S_2 and C_2 close to criticality for the QDKCA and the QBBR. We compute these quantities by simulating the reduced evolution of ρ_t using tensor networks (TNs) and matrix product states (MPSs) [38,39]. The method employed—detailed in Ref. [34]—relies on representing ρ_t as an MPS and $\mathcal{G}$ as a matrix product operator (MPO), and applying standard methods for simulating MPS evolution [40,41]. Details concerning the lattice size L, MPS bond-dimension χ and other parameters related to the simulation are contained in the caption of Fig. 2. All simulations start with an initial seed placed in the center of the first time slice [see Fig. 1(a)].

In Fig. 2(a) we show the entropy S_2 for the QDKCA with $p_2 = 0.874$ and the six values of p_1 indicated in the figure (solid lines). For the two lowest values of p_1, the second-order Renyi entropy rapidly vanishes, due to the fact that the systems approaches an absorbing (product) state. In contrast, the curves with the three highest values of p_1 tend to stationary values. This demonstrates that S_2 can play the role of an order parameter, by distinguishing between the two different phases. When choosing $p_2 = p_1(2 - p_1)$ the DKCA is equivalent to so-called bond-directed percolation and extensive studies of this classical process have determined the location of the critical point as $p_2 = 0.874$, $p_1 = 0.645$ [6]. The corresponding critical curve is shown as solid green lines in Figs. 2(a) and 2(b). Here, S_2 follows a power-law behavior. By fitting the curve between $t = [50, 200]$, we estimate the critical exponent to be $q_{\rm ent} = 0.213 \pm 0.004$.

Note that, in estimating critical exponents for APTs, determining the location of the critical point is typically a key source of error [6]. However, since the QDKCA and DKCA share the same critical point by construction, in our case this error is negligible. The relevant error sources for the QDKCA model are thus associated with finite-L, finite-χ, and finite-time effects. In contrast, due to the relatively few studies on the BBR model, for the QBBR model the uncertainty on the location of the critical point provides a significant contribution to the error. Overall, in addition to larger finite-χ errors, the error associated with the estimates of the critical exponents for the QBBR model are considerably larger than those of the QDKCA. For details on the estimation of errors, and a further discussion of related issues, see Ref. [34].

Figure 2(a) also displays $S_2^{\rm cl}$ (dashed lines). For each p_1, as t increases, the curves for S_2 and $S_2^{\rm cl}$ become indistinguishable on the scale shown. This means that the critical exponent found also holds for the classical model. We remark that this is different from the value obtained for $S_2^{\rm cl}$ in Ref. [11], which may be due to the fact that we are not using a homogeneous initial condition but an initial seed instead. The agreement between $S_2(t)$ and $S_2^{\rm cl}(t)$ suggests that C_2 becomes irrelevant compared with $\mathrm{Tr}[(\rho_t^{\rm cl})^2]$ over time [34]. This is confirmed in Fig. 2(b), where C_2 is shown

for the same values of p_1. As with S_2, at criticality we observe a power-law behavior in C_2. However, we find that the timescale over which C_2 approaches a power law is considerably larger than that of S_2. As such, to estimate the critical exponent, we construct the time-dependent effective exponent, $q_{\mathrm{coh}}(t) = -\ln[C_2(t)/C_2(t/2)]$, as shown in the inset of Fig. 2(b). As can be seen, C_2 does indeed approach a power-law [indicated by $q_{\mathrm{coh}}(t)$ approaching a constant value], and we estimate the exponent to be $q_{\mathrm{coh}} = 2.96 \pm 0.04$ by averaging over the effective exponent between $t = [450, 550]$.

Figures 2(c) and 2(d) display S_2 and C_2 for the QBBR model. In each case we set $p_2 = 0.2$ and choose six values for p_1 as indicated in the legend. When $p_1 = 0.610$ (solid green line) a power law can be observed, with estimated exponent $q_{\mathrm{ent}} = 0.27 \pm 0.07$, obtained by fitting a curve between $t = [50, 200]$. Moreover, as t increases, S_2 and S_2^{cl} become indistinguishable. This is explained by the decay of C_2, shown in Fig. 2(d). Using the effective exponent for $p_1 = 0.610$ (shown in the inset), we estimate $q_{\mathrm{coh}} = 2.74 \pm 0.27$, by averaging over $t = [150, 200]$.

Conclusions and outlook.—QCA constitute a platform that allows us to realize a number of canonical CA scenarios. They can be experimentally realized on quantum simulators [42,43] and encode the entire space-time information of a nonequilibrium process in a single quantum state. This permits experimental access to unusual properties, such as entanglement in the time domain [44]. Already simple QCA, which are quantum generalizations of the classical DKCA and the BBR model, reveal intriguing features, such as power-law scaling of entanglement and coherence with time at criticality. In the future it would be interesting to focus on more intricate situations, e.g., QCA where the elementary gates do not commute, so that the order in which local updates are applied defines inequivalent global updates $\mathcal{G}_t$ [18]. In such a setting, the updates in $(1+1)$D QCA can be considered as asynchronous updates, the impacts of which have been extensively studied in the classical case [45–47] but are still largely unexplored in the quantum domain.

We acknowledge support from Engineering and Physical Sciences Research Council [Grant No. EP/R04421X/1], from the "Wissenschaftler Rückkehrprogramm GSO/CZS" of the Carl-Zeiss-Stiftung and the German Scholars Organization e.V., as well as through The Leverhulme Trust [Grant No. RPG-2018-181], and the Deutsche Forschungsgemeinschaft through SPP 1929 (GiRyd), Grant No. 428276754, as well as through Grant No. 435696605. We are grateful for access to the University of Nottingham's Augusta high performance computing service.

[1] P. Grassberger and A. de la Torre, Ann. Phys. (N.Y.) **122**, 373 (1979).
[2] G. Ódor, Rev. Mod. Phys. **76**, 663 (2004).
[3] S. Lübeck, Int. J. Mod. Phys. B **18**, 3977 (2004).
[4] S. Wolfram, Rev. Mod. Phys. **55**, 601 (1983).
[5] S. Wolfram, *A New Kind of Science* (Wolfram Media Inc., Champaign, 2002).
[6] M. Henkel, H. Hinrichsen, and S. Lübeck, *Non-Equilibrium Phase Transitions* (Springer, Netherlands, 2008).
[7] E. Domany and W. Kinzel, Phys. Rev. Lett. **53**, 311 (1984).
[8] T. E. Harris, Ann. Probab. **2**, 969 (1974).
[9] K. A. Takeuchi, M. Kuroda, H. Chaté, and M. Sano, Phys. Rev. Lett. **99**, 234503 (2007).
[10] G. Lemoult, L. Shi, K. Avila, S. V. Jalikop, M. Avila, and B. Hof, Nat. Phys. **12**, 254 (2016).
[11] K. Harada and N. Kawashima, Phys. Rev. Lett. **123**, 090601 (2019).
[12] K. Wiesner, Quantum cellular automata, in *Encyclopedia of Complexity and Systems Science*, edited by R. A. Meyers (Springer, New York, New York, 2009), pp. 7154–7164.
[13] J. I. Cirac, D. Perez-Garcia, N. Schuch, and F. Verstraete, J. Stat. Mech. 08 (2017) 083105.
[14] P. Arrighi, Nat. Comput. **18**, 885 (2019).
[15] T. Farrelly, Quantum **4**, 368 (2020).
[16] L. E. Hillberry, M. T. Jones, D. L. Vargas, P. Rall, N. Yunger Halpern, N. Bao, S. Notarnicola, S. Montangero, and L. D. Carr, Quantum Sci. Technol. **6**, 045017 (2021).
[17] I. Lesanovsky, K. Macieszczak, and J. P. Garrahan, Quantum Sci. Technol. **4**, 02LT02 (2019).
[18] E. Gillman, F. Carollo, and I. Lesanovsky, Phys. Rev. Lett. **125**, 100403 (2020).
[19] M. Buchhold, B. Everest, M. Marcuzzi, I. Lesanovsky, and S. Diehl, Phys. Rev. B **95**, 014308 (2017).
[20] F. Carollo, E. Gillman, H. Weimer, and I. Lesanovsky, Phys. Rev. Lett. **123**, 100604 (2019).
[21] E. Gillman, F. Carollo, and I. Lesanovsky, New J. Phys. **21**, 093064 (2019).
[22] M. Jo, J. Um, and B. Kahng, Phys. Rev. E **99**, 032131 (2019).
[23] M. Jo and B. Kahng, Phys. Rev. E **101**, 022121 (2020).
[24] M. Jo, J. Lee, K. Choi, and B. Kahng, Phys. Rev. Research **3**, 013238 (2021).
[25] E. Gillman, F. Carollo, and I. Lesanovsky, Phys. Rev. A **103**, L040201 (2021).
[26] K. Beer, D. Bondarenko, T. Farrelly, T. J. Osborne, R. Salzmann, D. Scheiermann, and R. Wolf, Nat. Commun. **11**, 808 (2020).
[27] J. Zeiher, R. Van Bijnen, P. Schauß, S. Hild, J.-y. Choi, T. Pohl, I. Bloch, and C. Gross, Nat. Phys. **12**, 1095 (2016).
[28] H. Kim, Y. J. Park, K. Kim, H.-S. Sim, and J. Ahn, Phys. Rev. Lett. **120**, 180502 (2018).
[29] A. Browaeys and T. Lahaye, Nat. Phys. **16**, 132 (2020).
[30] S. Ebadi, T. T. Wang, H. Levine, A. Keesling, G. Semeghini, A. Omran, D. Bluvstein, R. Samajdar, H. Pichler, W. W. Ho *et al.*, arXiv:2012.12281.
[31] D. Petz, *Quantum Information Theory and Quantum Statistics* (Springer, Berlin, Heidelberg, 2008).
[32] F. Bagnoli, N. Boccara, and R. Rechtman, Phys. Rev. E **63**, 046116 (2001).
[33] H. Hinrichsen, Adv. Phys. **49**, 815 (2000).
[34] see Supplemental Material at http://link.aps.org/supplemental/10.1103/PhysRevLett.127.230502 for details on the calculations presented in the main text, the numerical methods used and the estimation of errors.

[35] T. Toffoli and N. H. Margolus, Physica (Amsterdam) **45D**, 229 (1990).
[36] F. Bagnoli and R. Rechtman, arXiv:1409.4284.
[37] T. Baumgratz, M. Cramer, and M. B. Plenio, Phys. Rev. Lett. **113**, 140401 (2014).
[38] U. Schollwöck, Ann. Phys. (Amsterdam) **326**, 96 (2011).
[39] S. Montangero, *Introduction to Tensor Network Methods* (Springer, Cham, 2018).
[40] S. Paeckel, T. Köhler, A. Swoboda, S. R. Manmana, U. Schollwöck, and C. Hubig, Ann. Phys. (Amsterdam) **411**, 167998 (2019).
[41] S.-J. Ran, E. Tirrito, C. Peng, X. Chen, G. Tagliacozzo, Luca Su, and M. Lewenstein, *Tensor Network Contractions* (Springer, Cham, 2020).
[42] P. Scholl, M. Schuler, H. J. Williams, A. A. Eberharter, D. Barredo, K.-N. Schymik, V. Lienhard, L.-P. Henry, T. C. Lang, T. Lahaye, A. M. Läuchli, and A. Browaeys, Nature (London) **595**, 233 (2021).
[43] S. Ebadi, T. T. Wang, H. Levine, A. Keesling, G. Semeghini, A. Omran, D. Bluvstein, R. Samajdar, H. Pichler, W. W. Ho, S. Choi, S. Sachdev, M. Greiner, V. Vuletić, and M. D. Lukin, Nature (London) **595**, 227 (2021).
[44] R. Islam, R. Ma, P. M. Preiss, M. Eric Tai, A. Lukin, M. Rispoli, and M. Greiner, Nature (London) **528**, 77 (2015).
[45] O. Bouré, N. Fatès, and V. Chevrier, Nat. Comput. **11**, 553 (2012).
[46] S. Bandini, A. Bonomi, and G. Vizzari, Nat. Comput. **11**, 277 (2012).
[47] N. Fatès, in *Cellular Automata and Discrete Complex Systems*, edited by J. Kari, M. Kutrib, and A. Malcher (Springer Berlin Heidelberg, Berlin, Heidelberg, 2013), pp. 15–30.